01 Mar 1994

Microwave Noncontact Examination of Disbond and Thickness Variation in Stratified Composite Media

Sasan Bakhtiari

Nasser N. Qaddoumi

Stoyan I. Ganchev

R. Zoughi
Missouri University of Science and Technology, zoughi@mst.edu

Recommended Citation

S. Bakhtiari et al., "Microwave Noncontact Examination of Disbond and Thickness Variation in Stratified Composite Media," *IEEE Transactions on Microwave Theory and Techniques*, vol. 42, no. 3, pp. 389-395, Institute of Electrical and Electronics Engineers (IEEE), Mar 1994.
The definitive version is available at https://doi.org/10.1109/22.277431

Microwave Noncontact Examination of Disbond and Thickness Variation in Stratified Composite Media

Sasan Bakhtiari, Nasser Qaddoumi, Stoyan I. Ganchev, and Reza Zoughi

Abstract—**Numerical and experimental results of a microwave noncontact, nondestructive detection and evaluation of disbonds and thickness variations in stratified composite media are presented. The aperture admittance characteristics of a flange mounted rectangular waveguide radiating into a layered, generally lossy dielectric media backed or unbacked by a conducting sheet is modeled. The theoretical implementation is based on a Fourier transform boundary matching technique to construct the field components in each medium, coupled with a stationary form of the terminating aperture admittance of the waveguide. The model can serve as a reliable test bed for real-time examination of layered composite media. Experimental results for several cases are presented which show good agreement with the theoretical findings. This is a versatile technique for near-field *in situ* interrogation of stratified composite media which provides for high resolution measurements.**

I. Introduction

NONCONTACT nondestructive evaluation (NDE) of disbonds, delaminations and minute thickness variations in stratified composite materials is of great interest in many industrial applications. Good examples would be thickness variations, disbonds and delamination detection in ceramic, synthetic rubber, and honeycomb composite structures. In many instances, the layered structure is backed by a conducting plate, or it is a dielectric coating on top of a conducting sheet. Noncontact microwave NDE techniques have demonstrated tremendous potential in such applications although they have not received the acknowledgement of other conventional techniques such as ultrasonic, eddy currents, and X-rays. The ability of microwaves to penetrate inside a dielectric medium and their sensitivity to the presence of a boundary between two dissimilar layers make them suitable for this type of measurements [1]–[3].

Much work has been done on rigorous theoretical analysis of a rectangular waveguide radiating into a layered media. The applications at which these works have been aimed at are just as diverse. Most of the earlier literature have addressed the problem of plasma covered aperture antennas [4]–[7]. More recent rigorous analysis have been presented mostly in application to measurement of dielectric properties of materials and field interactions with biological tissues [8]–[12]. Considering typical measurement resolutions and accuracies in near-field examination of generally lossy composite media, most rigorous numerical results offer little practical advantage when taking into account the necessary computation time and difficulties involved in replicating the results by means of well-controlled experimental setups.

The approach adopted here was originally applied in [6] in application to radiation from plasma covered aperture antennas. It is assumed that the aperture field distribution is that of the dominant mode. This approach was first implemented and tested for the practical case of thickness measurement and variation detection of lossy dielectric slabs backed by a conducting plate [13]. In this work the solution is expanded to include general N-layer stratified dielectric media which may be terminated by a conducting sheet or an infinite half-space. This is done using a Fourier transform boundary matching technique to construct the field solutions in the layered medium outside the waveguide. A variational expression for the terminating aperture admittance in an infinite ground plane is used to construct the desired solution. Furthermore, the numerical results have been compared with several experimental measurements using a precise mechanical device built specifically for this purpose. Some important observations regarding both the numerical and experimental results have been acknowledged.

Manuscript received October 7, 1992; revised May 10, 1993.

The authors are with the Applied Microwave Nondestructive Testing Laboratory, Electrical Engineering Department, Colorado State University, Ft. Collins, CO 80523.

IEEE Log Number 9215158.

II. Theoretical Formulation

Fig. 1 shows a rectangular aperture in an infinite flange. Variational expression for the terminating admittance of the waveguide can be written as [6]

$$Y = G + jB = \frac{\iint_{\text{aperture}} \left[\overline{E}(x,y,0) \times \overline{W}(x,y)\right] \cdot \hat{a}_z dx\, dy}{\left[\iint_{\text{aperture}} \overline{E}(x,y,0) \cdot \overline{e}_0(x,y) dx\, dy\right]^2} \tag{1}$$

where,

$$\overline{W}(x,y) = \overline{H}(x,y,0) + \sum_{i=1}^{\infty} Y_i \overline{h}_i(x,y) \iint_{\text{aperture}} \overline{E}(\eta,\xi,0) \cdot \overline{e}_i(\eta,\xi) d\eta d\xi \tag{2}$$

and $\overline{E}(x,y,0)$ and $\overline{H}(x,y,0)$ represent the aperture field distributions. G and B are the aperture conductance and susceptance respectively. This admittance expression is constructed using transverse vector mode functions and their orthogonal properties [14]. $\overline{e_i}$ and $\overline{h_i}$ are the ith vector mode functions and Y_i is the characteristic admittance of the the

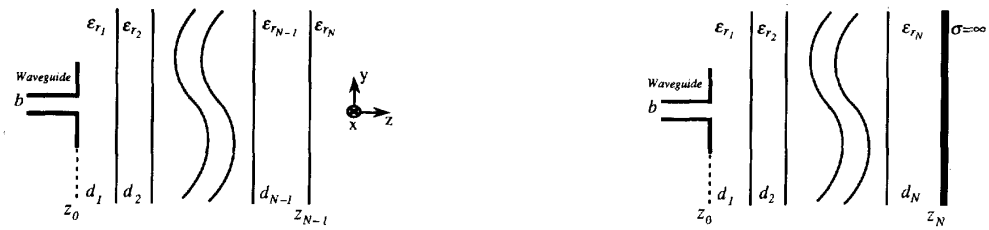

Fig. 1. Cross section of an N-layer stratified medium terminated by (a) an infinite half-space (b) a conducting plate.

ith waveguide mode. It has been shown that (1) is stationary with respect to variations of the aperture E-field about its exact value [6], [15], [16]. Thus, a resonable approximation for the electric field results in a good estimate of the aperture admittance. It must be noted that as standard practice, a square flange with sides greater than $1\lambda_0$ is a good approximation to the theoretical assumption of an infinite flange for near-field measurements [17].

With the TE_{10} mode incident on the aperture, a symmetrical electric field distribution over the large dimension can be written as

$$E_y(x,y,0) = \bar{e}_0(x,y) = \begin{cases} \sqrt{\frac{2}{ab}}\cos\left(\frac{\pi x}{a}\right) & \text{Over Aperture} \\ 0 & \text{Elsewhere} \end{cases} \quad (3)$$

where a and b are the large and small dimensions of the waveguide cross section respectively, and the distribution is normalized so that a Fourier transform boundary matching technique is used to construct the field solutions in an N-layer stratified generally lossy dielectric medium. The transverse field components are expanded in each layer in terms of Fourier integrals. Subsequently, appropriate boundary conditions across each interface is enforced to solve for the unknown field coefficients in each medium. Fig. 1(a) and (b) depict the cross section of an open-ended waveguide radiating into a layered medium which is terminated into an infinite half-space and a perfect conducting sheet respectively. Each layer is assumed to be homogeneous and nonmagnetic with relative complex dielectric constant ε_{r_n}.

The fields outside the waveguide may be constructed using a single vector potential. In each layer, denoted by layer number n, fields must satisfy the source-free wave equation

$$\overline{E}^n(x,y,z) = -\nabla \times \overline{\Pi}^n \quad (4a)$$

$$\overline{H}^n(x,y,z) = \frac{1}{j\omega\mu_0}\left[k_n^2\overline{\Pi}^n + \nabla\nabla\cdot\overline{\Pi}^n\right] \quad (4b)$$

where, $\overline{\Pi}^n = \Phi_n\hat{a}_x + \Psi_n\hat{a}_y$.

General solutions of (4a) and (4b) may be expressed in terms of integrations over the entire mode space as

$$\mathbf{E}^n_{\left\{\begin{smallmatrix}x\\y\end{smallmatrix}\right\}}(x,y,z) = \frac{jk_{z_n}}{(2\pi)^2}\int_{-\infty}^{\infty}\int_{-\infty}^{\infty} \left[\mp A^+_{\left\{\begin{smallmatrix}\Psi_n\\\Phi_n\end{smallmatrix}\right\}}e^{-jk_{z_n}z} \pm A^-_{\left\{\begin{smallmatrix}\Psi_n\\\Phi_n\end{smallmatrix}\right\}}e^{jk_{z_n}z}\right] e^{-j(k_xx+k_yy)}dk_xdk_y \quad (5a)$$

$$\mathbf{H}^n_{\left\{\begin{smallmatrix}x\\y\end{smallmatrix}\right\}}(x,y,z) = \frac{1}{(2\pi)^2}\int_{-\infty}^{\infty}\int_{-\infty}^{\infty}\frac{1}{j\omega\mu_0}\left\{\left[k_n^2 - k^2_{\left\{\begin{smallmatrix}x\\y\end{smallmatrix}\right\}}\right] \left[A^+_{\left\{\begin{smallmatrix}\Phi_n\\\Psi_n\end{smallmatrix}\right\}}e^{-jk_{z_n}z} + A^-_{\left\{\begin{smallmatrix}\Phi_n\\\Psi_n\end{smallmatrix}\right\}}e^{jk_{z_n}z}\right] - k_xk_y\left[A^+_{\left\{\begin{smallmatrix}\Psi_n\\\Phi_n\end{smallmatrix}\right\}}e^{-jk_{z_n}z} + A^-_{\left\{\begin{smallmatrix}\Psi_n\\\Phi_n\end{smallmatrix}\right\}}e^{jk_{z_n}z}\right]\right\} e^{-j(k_xx+k_yy)}dk_xdk_y \quad (5b)$$

where k_n is the complex propagation constant for the nth layer, and

$$k_{z_n} = \sqrt{k_n^2 - k_x^2 - k_y^2} \quad (6)$$

is taken as $k_{z_n} = |\mathrm{Re}\{k_{z_n}\}| - j|\mathrm{Im}\{k_{z_n}\}|$ to comply with the appropriate direction of propagation. Referring to Fig. 1(a), only positively travelling waves exist in the Nth layer which is unbounded in $+z$ direction. Thus, for the the field components in this region only those terms in (5a) and (5b) which are associated with positive direction of propagation remain. Using Fourier properties of the field components in (5) and enforcing the continuty of the tangential field components at each interface, the unknown field coefficients for each layer can be determined. Following the treatment given in the Appendix, the admittance expression (A8) once normalized with respect to guide admittance can be expressed as

$$y_s = g_s + jb_s = \frac{j2}{(2\pi)^2\sqrt{1-\left(\frac{\pi}{a'}\right)^2}}\int_{\mathcal{R}=0}^{\infty}\int_{\theta=0}^{\pi} \left\{[\varepsilon_{r_1} - (\mathcal{R}\cos\theta)^2]\left(2\mathcal{A}^+_{\Phi_1} + \frac{j\mathcal{G}(\mathcal{R},\theta)}{\sqrt{\varepsilon_{r_1}-\mathcal{R}^2}}\right) - 2\mathcal{R}^2\sin\theta\cos\theta\mathcal{A}^+_{\Psi_1}\right\}\mathcal{G}(\mathcal{R},\theta)\mathcal{R}\ d\theta\ d\mathcal{R} \quad (7)$$

where,

$$\mathcal{G}(\mathcal{R},\theta) = \sqrt{\frac{2a'}{b'}}\frac{(4\pi)\cos\left(\frac{a'\mathcal{R}\cos\theta}{2}\right)\sin\left(\frac{b'\mathcal{R}\sin\theta}{2}\right)}{(\mathcal{R}\sin\theta)[\pi^2 - (a'\mathcal{R}\cos\theta)^2]} \quad (8)$$

with $\mathcal{R}$ and θ as the new variables of integration given by (A9) and a' and b' are the normalized waveguide dimensions. Calculation of the normalized field coefficients $\mathcal{A}^+_{\Phi_1}$ and $\mathcal{A}^+_{\Psi_1}$ in (7) is outlined in the Appendix. Lossless stratified media is not the focus of this work, however, for such a case one encounters singularities in (7). This can be resolved by contour integration around singular points of the integrand located on

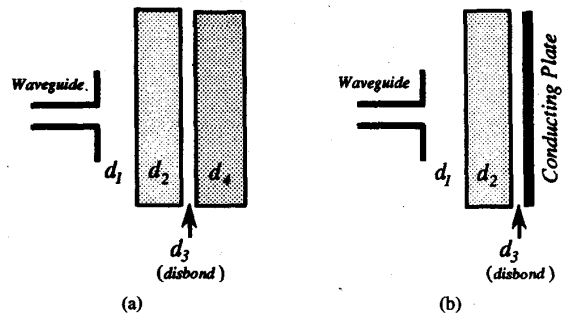

Fig. 2. Cross sectional geometries for the measurement setup. (a) termination into free-space (b) termination into a conducting sheet.

the real axis and take into account the residue. In application to a composite medium which contains generally lossy layers, which is the case addressed here, the poles of the integrand move off of the real axis and the integrand becomes smooth. This allows quick and efficient numerical integration schemes such as a Gauss quadrature method (used here) to be applied.

III. Theoretical and Experimental Results and Observations

The complex reflection coefficient, R is related to normalized complex admittance, y_s, by $R = (1 - y_s)/(1 + y_s)$. Thus, the magnitude and phase of R can be measured directly from VSWR and shift in the location of the standing wave null compared to a short circuited waveguide [18]. The apparatus utilized to conduct experimental measurements incorporated a slotted line and a mechanical setup with two sliding sample holders which allowed precise adjustment of the sample positions, via two micrometers, in front of the waveguide aperture. Fig. 2(a) and (b) depict the two basic geometries examined by this apparatus. The measurements presented here were performed at a frequency of 10 GHz using dielectric sheets with permittivity and loss tangent of $\varepsilon_r' = 8.4$ and $\tan\delta = 0.107$ (synthetic rubber sheets). The experimental results presented here are the average value of several independent measurements.

A. Termination of Layered Media into an Infinite Half-Space

To examine the validity and limitations of the numerical results, initially variations of VSWR and phase were monitored as a function of distance between the aperture and the sample (air gap) using a single slab terminated into free-space. The geometry configuration of the measurement is derived from Fig. 2(a) with a dielectric sample thickness of $d_2 = 7.55$ mm, and with d_3 and d_4 equal to zero. The measured slab thickness using a micrometer thickness gauge, is the mean value over the aperture area. The results of the theoretical and measured VSWR and phase for a range of air gap values are shown in Fig. 3 over a distance of $\lambda_o/2$ from the aperture. There is a good agreement between the measurement and numerical results. As expected, the air gap size dictates the degree of the field coupling into the dielectric slab and can be manipulated for measurement purposes.

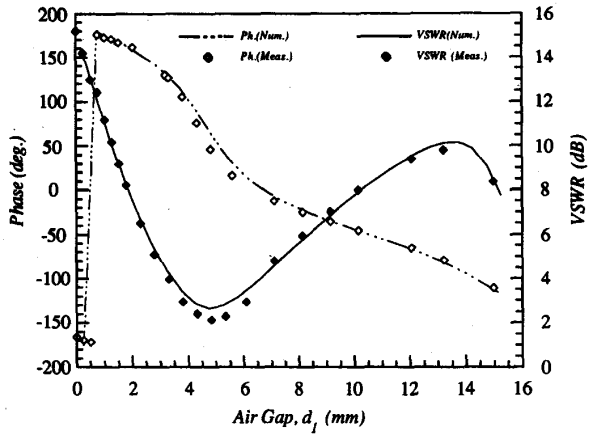

Fig. 3. Comparison of numerical and experimental results for VSWR and phase as a function of air gap d_1 for a two layer media terminated into free-space.

Next, variations of VSWR and phase were investigated as a function of the slab thickness for a fixed arbitrary air gap distance d_1. Once again Fig. 2(a) illustrates the geometry for this case with d_3 and d_4 equal to zero. Figs. 4 and 5 show the numerical results at 24 GHz along with both the numerical and experimental results at 10 GHz for different slab thicknesses. Figs. 4(a) and (b) show variations of VSWR and phase respectively for an air gap of $d_1 = 2$ mm. The numerical results of phase variation at 24 GHz shows a change of around 120 degrees over the first 4.5 mm range of slab thickness. This indicates that for this case thickness variations as small as 0.04 mm may be detected since the measurement apparatus used here may resolve a change of one degree. Figs. 5(a) and (b) display the results for an air gap of $d_1 = 5$ mm. The measured phase at 10 GHz, which is also predicted by the theory, shows significant variation over this thickness range. Due to greater signal attenuation at larger air gaps and increase in electrical length of the lossy sample at higher frequencies, variations of VSWR and phase are expected to degrade as shown for the 24 GHz results in Fig. 5. Such observations are made to indicate that the measurement resolution (accuracy) may be maximized by using the theory to optimize the air gap distance and the operating frequency based on the sample thickness and its dielectric properties. Moreover, having such resolutions at X-band suggests that one may not need to go to much higher frequencies to achieve high resolutions for examination of the type of dielectric samples used here, although higher frequencies may eventually render better accuracies for thin and low-loss materials.

To examine the effect of disbond in a stratified composite medium an experiment was conducted in which the separation between two slabs of the same dielectric material (disbond) was varied for a fixed air gap. Once again, Fig. 2(a) depicts the geometry of this case for $d_2 = 5.15$ mm, $d_4 = 7.55$ mm, and with both slabs having the same dielectric constant as before. Layers 1, 3, and the infinite half-space in the back have free-space permittivity. Fig. 6 shows the numerical and experimental results for $d_1 = 5$ mm as d_3 varies over a

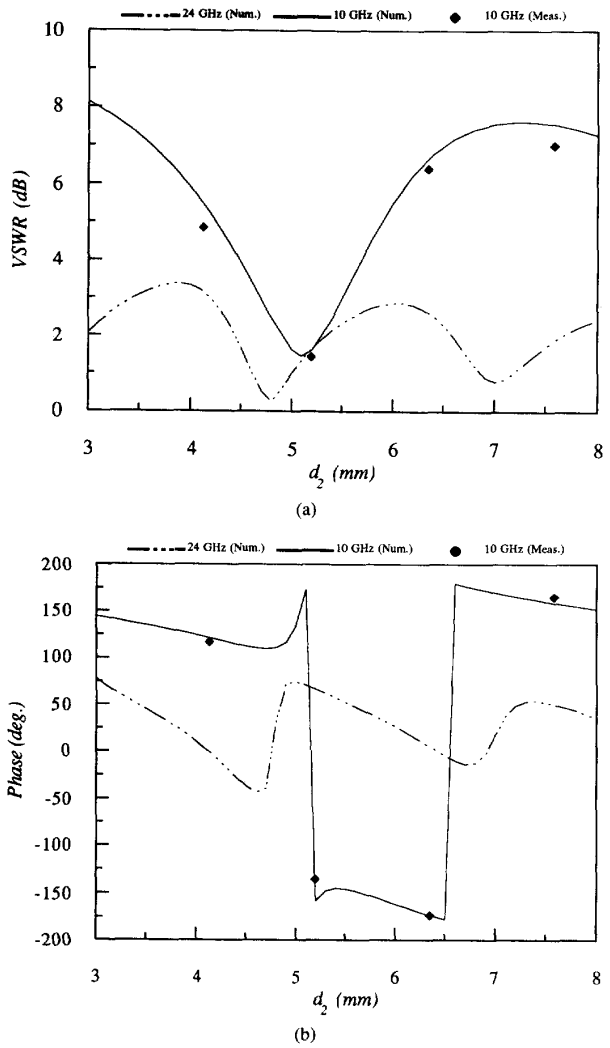

Fig. 4. (a) Comparison of numerical results at 10 and 24 GHz along with experimental results at 10 GHz for VSWR as a function of slab thickness for an arbitrary air gap of $d_1 = 2$ mm. (b) Comparison of numerical results at 10 and 24 GHz along with experimental results at 10 GHz for phase as a function of slab thickness for an arbitrary air gap of $d_1 = 2$ mm.

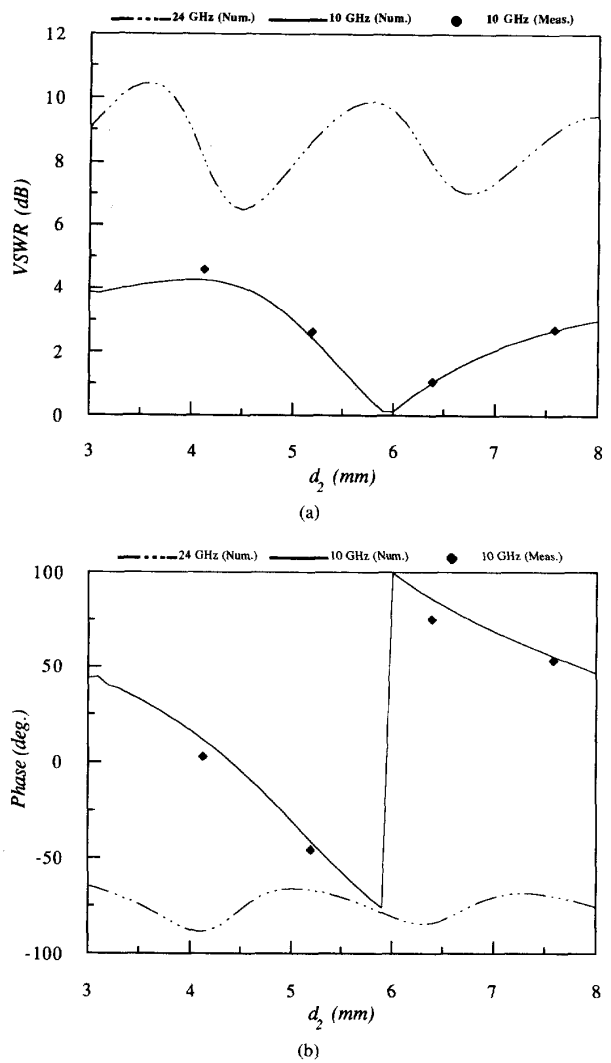

Fig. 5. (a) Comparison of numerical results at 10 and 24 GHz along with experimental results at 10 GHz for VSWR as a function of slabthickness d_2 for an arbitrary air gap of $d_1 = 5$ mm. (b) Comparison of numerical results at 10 and 24 GHz along with experimental results at 10 GHz for phase as a function of slab thickness d_2 for an arbitrary air gap of $d_1 = 5$ mm.

$\lambda_0/10$ range. The measurement outcomes, which are in good agreement with the theory, clearly indicate that for this specific case, the phase of the reflection coefficient shows much more sensitivity to the disbond dimension than VSWR. The phase drops around 15 degrees over the first 0.5 mm variation of disbond in the layered medium.

B. Termination of Layered Media into a Conducting Sheet

Similar measurements were performed for the case where the medium is backed by a conducting plate. Referring to Fig. 2(b), a slab with thickness of $d_2 = 7.55$ mm was first placed flush against a metal plate ($d_3 = 0$), and d_1 varied over a $\lambda_0/2$ distance. The numerical and experimental results for VSWR and phase are shown in Fig. 7. Comparing VSWR in Fig. 7 with its counterpart in Fig. 3 where the conductor is not present one can clearly observe the effect of strong reflection from the surface of the metal plate causing slower damping of the VSWR variation in Fig. 7. Similarly comparison between phase of these two cases shows the strong influence of the conductor backing both in terms of a shift in position and change of slope in the phase variation.

Fig. 8 displays variations of VSWR and phase as a function of disbond thickness variation, d_3, between the dielectric sheet and the metal plate for an air gap of $d_1 = 5$ mm. Both VSWR and phase values, which are in close agreement with the theory, display significant change over the $\lambda_0/10$ range. Comparing the phase shown in Fig. 8 with that of Fig. 7, it is clear that the presence of the conducting sheet in the back enhances the measurement sensitivity. Such an

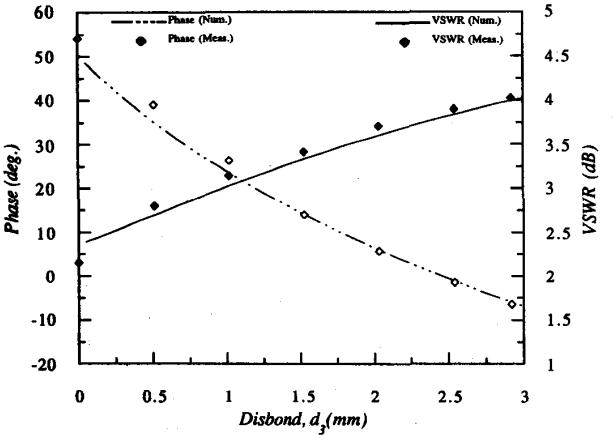

Fig. 6. Comparison of numerical and experimental results for VSWR and phase as a function of disbond d_3. $d_1 = 5$ mm, $d_2 = 5.15$ mm, $d_4 = 7.55$ mm.

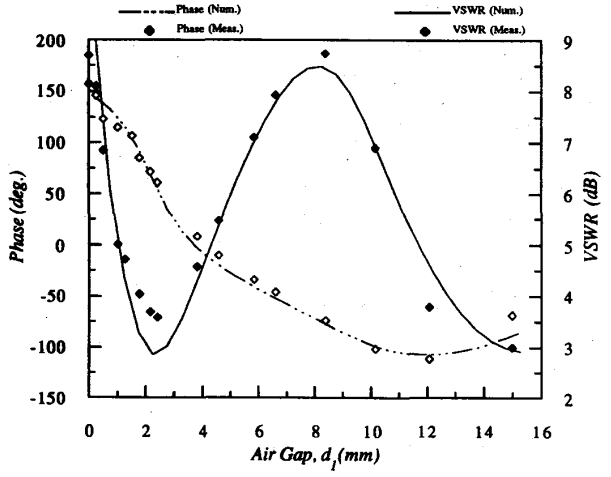

Fig. 7. Comparison of numerical and experimental results for VSWR and phase as a function of d_1.$d_2 = 7.55$ mm, $d_3 = 0$.

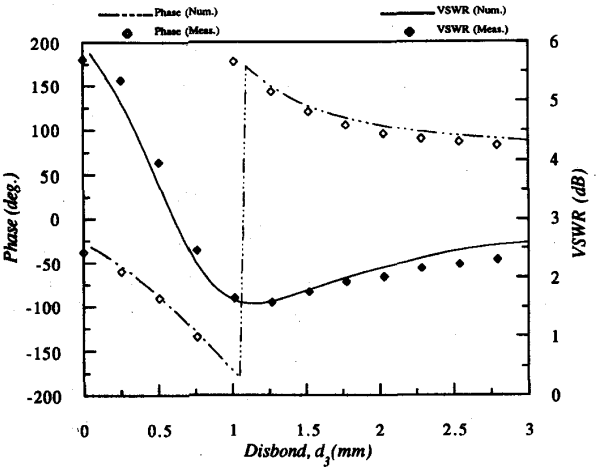

Fig. 8. Comparison of numerical and experimental results for VSWR and phase as a function of d_3. $d_1 = 5$ mm, $d_2 = 7.55$ mm.

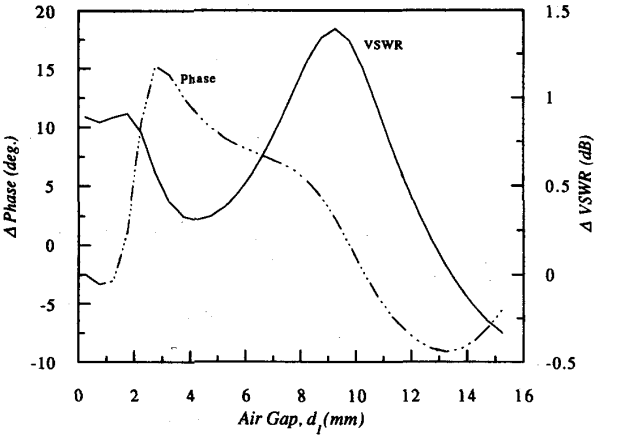

Fig. 9. Difference between the numerical results of Fig. 5 with the case were a small disbond of $d_3 = 0.1$ mm is also present.

effect is expected due to a strong reflection at the interface between the dielectric slab and the surface of conducting plate. These results clearly illustrate the utility of this approach for detecting a disbond at its early stages of development.

To further stress the effect of air gap on the measurement resolution, the numerical results of VSWR and phase of Fig. 7 (disbond $d_3 = 0$) were compared against a case where a disbond of $d_3 = 0.1$ mm exists between the dielectric sheet and the metal plate. The results of this test are shown in Fig. 9. The solid line displays the difference between the magnitude of VSWR (in dB) and the dashed line is the phase difference between the two cases. The results clearly indicate a resolvable difference as a result of a 0.1 mm disbond between the dielectric slab and the conductor surface. The maximum difference of the VSWR and phase occurs at different air gaps. Such tests demonstrate that the theory may render important information on the air gap for the position of maximum separation of either the VSWR or the phase for optimization of measurement resolution and accuracy.

IV. Conclusion

A theoretical model along with experimental results have been presented in application to microwave *in situ* NDE of layered dielectric media terminating into either free-space or a conducting sheet. The theoretical analysis is based on a Fourier transform boundary matching technique to construct the field components in a layered media outside an open-ended rectangular waveguide coupled with the variational form of the terminating admittance of the flange-mounted aperture. The integrity of the numerical results have been examined by conducting several measurements using a precise mechanical device built specifically to duplicate the geometry of the theoretical model. The measurements presented here were performed at 10 GHz using generally lossy slab-like samples. Variation of VSWR and phase of the reflection coefficient

as a function of parameters such as the air gap between the sample and the waveguide, and sample thickness were investigated. Furthermore, numerical and experimental results were presented demonstrating the possibility for detection of small disbond thicknesses in a layered media. The experimental results showed good agreement with the numerical outcomes. These results clearly indicate that high resolutions may be achieved in examination of generally lossy dielectric samples without the need to operate at very high frequencies. Furthermore, they demonstrate the sensitivity of such versatile NDE technique as it applies to the interrogation of layered composite media, and the importance of a fast and reliable numerical model as a tool to gain real time *a priori* knowledge of the underlying process. It is concluded that the theoretical model can render important information for optimization of such measurement parameters as position of the sensor and operating frequency leading to better resolutions.

APPENDIX

The boundry value problem was solved by introducing the following normalized (with respect to k_0) parameters inside the formulation

$$a' = k_0 a, b' = k_0 b, Z_n = k_0 \sum_{i=1}^{n} d_i, \mathcal{A}_I^{\pm} = k_0^2 A_I^{\pm}$$

$$\mathcal{K}_{x,y} = \frac{k_{x,y}}{k_0}, \mathcal{K}_n = \frac{k_{z_n}}{k_0} = \sqrt{\varepsilon_{r_n} - \mathcal{K}_x^2 - \mathcal{K}_y^2} \tag{A1}$$

where $n = 1, 2, \ldots N$, d_i is the thickness of the i^{th} layer, and the index I refers to Ψ or Φ component of the vector potential. Taking inverse transform of both components of (5a) at the aperture results in the following relations between the field coefficients in layer 1

$$\mathcal{A}_{\Psi_1}^{+} = \mathcal{A}_{\Psi_1}^{-} \tag{A2}$$

$$\mathcal{A}_{\Phi_1}^{+} - \mathcal{A}_{\Phi_1}^{-} = \frac{4\pi}{jk_1}\sqrt{\frac{2a'}{b'}}\frac{\cos\left(\frac{\mathcal{K}_x a'}{2}\right)\sin\left(\frac{\mathcal{K}_y b'}{2}\right)}{\mathcal{K}_y[\pi^2 - (\mathcal{K}_x a')^2]} = \frac{\mathcal{G}(\mathcal{K}_x, \mathcal{K}_y)}{jk_1} \tag{A3}$$

where $\mathcal{G}$ is chosen to simplify the notation. Forcing the appropriate boundary conditions, namely continuity of the transverse E and H-field components across each interface and vanishing tangential E-field over the conducting surface results in the following set of relations between the field coefficients of adjacent layers

$$\begin{aligned}
&\mathcal{A}^{+}_{\left\{\begin{smallmatrix}\Psi_m\\ \Phi_m\end{smallmatrix}\right\}} e^{-j\mathcal{K}_m z_m} - \mathcal{A}^{-}_{\left\{\begin{smallmatrix}\Psi_m\\ \Phi_m\end{smallmatrix}\right\}} e^{j\mathcal{K}_m z_m} \\
&= \frac{\mathcal{K}_{m+1}}{\mathcal{K}_m}\left[\mathcal{A}^{+}_{\left\{\begin{smallmatrix}\Psi_{m+1}\\ \Phi_{m+1}\end{smallmatrix}\right\}} e^{-j\mathcal{K}_{m+1} z_m} - \mathcal{A}^{-}_{\left\{\begin{smallmatrix}\Psi_{m+1}\\ \Phi_{m+1}\end{smallmatrix}\right\}} e^{j\mathcal{K}_{m+1} z_m}\right] \\
&\left(\varepsilon_{r_m} - \mathcal{K}^2_{\left\{\begin{smallmatrix}x\\ y\end{smallmatrix}\right\}}\right)\left[\mathcal{A}^{+}_{\left\{\begin{smallmatrix}\Phi_m\\ \Psi_m\end{smallmatrix}\right\}} e^{-j\mathcal{K}_m z_m} + \mathcal{A}^{-}_{\left\{\begin{smallmatrix}\Phi_m\\ \Psi_m\end{smallmatrix}\right\}} e^{j\mathcal{K}_m z_m}\right] \\
&- (\mathcal{K}_x\mathcal{K}_y)\left[\mathcal{A}^{+}_{\left\{\begin{smallmatrix}\Psi_m\\ \Phi_m\end{smallmatrix}\right\}} e^{-j\mathcal{K}_m z_m} + \mathcal{A}^{-}_{\left\{\begin{smallmatrix}\Psi_n\\ \Phi_m\end{smallmatrix}\right\}} e^{j\mathcal{K}_m z_m}\right]
\end{aligned} \tag{A4}$$

$$\begin{aligned}
&= \left(\varepsilon_{r_{m+1}} - \mathcal{K}^2_{\left\{\begin{smallmatrix}x\\ y\end{smallmatrix}\right\}}\right) \\
&\times \left[\mathcal{A}^{+}_{\left\{\begin{smallmatrix}\Phi_{m+1}\\ \Psi_{m+1}\end{smallmatrix}\right\}} e^{-j\mathcal{K}_{m+1} z_m} + \mathcal{A}^{-}_{\left\{\begin{smallmatrix}\Phi_{m+1}\\ \Psi_{m+1}\end{smallmatrix}\right\}} e^{j\mathcal{K}_{m+1} z_m}\right] \\
&- (\mathcal{K}_x\mathcal{K}_y)\left[\mathcal{A}^{+}_{\left\{\begin{smallmatrix}\Psi_{m+1}\\ \Phi_{m+1}\end{smallmatrix}\right\}} e^{-j\mathcal{K}_{m+1} z_n} + \mathcal{A}^{-}_{\left\{\begin{smallmatrix}\Psi_{m+1}\\ \Phi_{m+1}\end{smallmatrix}\right\}} e^{j\mathcal{K}_{m+1} z_m}\right]
\end{aligned} \tag{A5}$$

where $m = 1, 2, \ldots, (N-1)$ is the layer number. Consequently, when the medium is terminated into an infinite half-space the contribution of negative travelling field components drops out of (A4) and (A5). For a layered media terminating into a conducting sheet, the vanishing tangential E-field components over the conductor surface renders an additional set of relations between the field coefficients in the Nth layer as

$$\mathcal{A}^{-}_{\left\{\begin{smallmatrix}\Psi_N\\ \Phi_N\end{smallmatrix}\right\}} = e^{-j2\mathcal{K}_N z_N}\mathcal{A}^{+}_{\left\{\begin{smallmatrix}\Psi_N\\ \Phi_N\end{smallmatrix}\right\}} \tag{A6}$$

Solving simultaneously a system of $4N-2$ equations for the N-layered case terminated into an infinite half-space results in the sought for field coefficients. Similarly, a system of $4N$ equations has to be solved for the case of N-layer medium terminated into a conducting sheet. Application of Parseval's theorem allows the construction of the numerator of admittance expression (1) as

$$\begin{aligned}
&\int_{-\infty}^{\infty}\int_{-\infty}^{\infty}\left[\overline{E}(x,y,0) \times \overline{W}(x,y,0)\right]\cdot \hat{a}_z dxdy \\
&\qquad = \frac{1}{(2\pi)^2}\int_{-\infty}^{\infty}\int_{-\infty}^{\infty} E_y^{1^*}(k_x,k_y)\mathcal{H}_x^1(k_x,k_y)dk_x dk_y
\end{aligned} \tag{A7}$$

where the E and $\mathcal{H}$ on the right hand side of (A7) are the transformed field components of layer 1 from (5a) and (5b) and * represents the complex conjugate notation. Upon calculation of the field coefficients in layer 1 and use of (A7) the following admittance expression results from (1)

$$\begin{aligned}
Y_n = \frac{j}{(2\pi)^2}&\int_{-\infty}^{\infty}\int_{-\infty}^{\infty} \\
&\left\{[\varepsilon_{r_1} - \mathcal{K}_x^2]\left[2\mathcal{A}_{\Phi_1}^{+} + \frac{j\mathcal{G}(\mathcal{K}_x,\mathcal{K}_y)}{\mathcal{K}_1}\right] - 2\mathcal{K}_x\mathcal{K}_y\mathcal{A}_{\Psi_1}^{+}\right\} \\
&\mathcal{G}(\mathcal{K}_x,\mathcal{K}_y)d\mathcal{K}_x d\mathcal{K}_y
\end{aligned} \tag{A8}$$

where subscript n denotes normalization with respect to the free-space characteristic admittance. By applying a polar coordinate transformation of the form

$$\mathcal{K}_x = \mathcal{R}\cos\theta, \quad \mathcal{K}_y = \mathcal{R}\sin\theta \tag{A9}$$

with transformation Jacobian $\mathcal{R}$ to (A8), which has two infinite integrals, the terminating aperture admittance may be evaluated by a double integral having only one unbounded range of integration as given by (7).

ACKNOWLEDGMENT

This research was supported and the samples and part of the measurement apparatus were provided by the Gates Rubber Co., Denver, Colorado.

REFERENCES

[1] R. Zoughi and S. Bakhtiari, "Microwave nondestructive detection and evaluation of disbonding and delamination in layered dielectric slabs," *IEEE Trans. Instrum. Meas.*, vol. 39, pp. 157–168, Dec. 1990.

[2] R. Zoughi, J. Edwards, and S. Bakhtiari, "Swept microwave frequency nondestructive detection and evaluation of delamination in stratified dielectric media," *J. Wave-Material Interaction*, vol. 7, no. 1, pp. 427–438, Jan. 1992.

[3] S. Bakhtiari and R. Zoughi, "Microwave thickness measurement of lossy layered dielectric slabs using incoherent reflectivity," *Res. Nondestructive Eval.*, vol. 2, no. 4, pp. 195–205, 1990.

[4] J. Galejs, "Admittance of a Waveguide Radiating into Stratified Plasma," *IEEE Trans. Antennas Propagat.*, vol. AP-13, pp. 64–70, Jan. 1965.

[5] A. T. Villeneuve, "Admittance of waveguide radiating into plasma environment," *IEEE Trans. Antennas Propagat.*, vol. AP-13, pp. 115–121, Jan. 1965.

[6] R. T. Compton, "The admittance of aperture antennas radiating into lossy media," Ph.D. dissertation, Ohio State Univ., Columbus, 1964.

[7] W. F. Croswell, W. C. Taylor, C. T. Swift, and A. R. Cockrell, "The input admittance of rectangular waveguide-fed aperture under an inhomogeneous plasma: Theory and experiment," *IEEE Trans. Antennas and Propagat.*, vol. AP-16, pp. 475–487, July 1968.

[8] V. Teodoridis, T. Sphicopoulos, and F. E. Gardiol, "The reflection from an open ended rectangular waveguide terminated by layered dielectric medium," *IEEE Trans. Microwave Theory Tech.*, vol. MTT-33, May 1985.

[9] A. R. Jamieson and T. E. Rozzi, "Rigorous analysis of crosspolarization in flangemounted waveguide radiators," *Electron. Lett.*, vol. 13, pp. 742–744, Nov. 24, 1977.

[10] M. C. Decreton and F. E. Gardiol, "Simple nondestructive method for measurement of complex permittivity," *IEEE Trans. Instrum. Meas.*, vol. IM-23, pp. 434–438, Dec. 1974.

[11] R. H. MacPhie and A. I. Zaghloul, "Radiation from a rectangular waveguide with infinite flange—Exact solution by the correlation matrix method," *IEEE Trans. Antennas Propagat.*, vol. AP-28, pp. 497–503, July 1980.

[12] K. S. Nikita and N. K. Uzunoglu, "Analysis of the power coupling from a waveguide hyperthermia applicator into a three-layered tissue model," *IEEE Trans. Microwave Theory Tech.*, vol. 37, pp. 1794–1801, Nov. 1989.

[13] S. Bakhtiari, S. Ganchev, and R. Zoughi, "Open-Ended rectangular waveguide for nondestructive thickness measurement and variation detection of lossy dielectric slabs backed by a conducting plate," *IEEE Trans. Instrum. Meas.*, vol. 42, pp. 19–24, Feb. 1993.

[14] R. F. Harrington, *Time Harmonic Electromagnetic Fields.* New York: McGraw-Hill, 1961, p. 381.

[15] R. E. Collin, *Field Theory of Guided Waves.* New York: McGraw-Hill, 1960.

[16] J. Galejs, *Antennas in Inhomogeneous Media.* Elmstord, NY: Pergamon Press, 1969.

[17] W. F. Croswell, R. G. Rudduck, and D. M. Hatcher, "Admittance of a rectangular waveguide radiating into a dielectric slab," *IEEE Trans. Antennas Propagat.*, vol. AP-15, no. 5, pp. 627–633, Sept. 1967.

[18] S. Ganchev, S. Bakhtiari, and R. Zoughi, "A novel numerical technique for dielectric measurement of lossy dielectrics," *IEEE Trans. Instrum. Meas.*, vol. 41, pp. 361–365, June 1992.

Sasan Bakhtiari, for a photograph and biography see page 24 of the January issue of this TRANSACTIONS.

Nasser Qaddoumi, for a photograph and biography see page 24 of the January issue of this TRANSACTIONS.

Stoyan I. Ganchev (M'92–SM'92), for a photograph and biography see page 23 of the January issue of this TRANSACTIONS.

Reza Zoughi (M'87–SM'93), for a photograph and biography see page 24 of the January issue of this TRANSACTIONS.